BIOCHEMISTRY
including biophysical chemistry & molecular biology
Article

Biochemistry **2010,** *49,* 8155–8168 8155
DOI: 10.1021/bi100286n

Comparisons between Chemical Mapping and Binding to Isoenergetic Oligonucleotide Microarrays Reveal Unexpected Patterns of Binding to the *Bacillus subtilis* RNase P RNA Specificity Domain[†]

Ruiting Liang,[‡] Elzbieta Kierzek,[§] Ryszard Kierzek,[§] and Douglas H. Turner*[,‡]

[‡]*Department of Chemistry, University of Rochester, Rochester, New York 14627, and* [§]*Institute of Bioorganic Chemistry, Polish Academy of Sciences, 60-714 Poznan, Noskowskiego 12/14, Poland*

Received February 25, 2010; Revised Manuscript Received June 16, 2010

ABSTRACT: Microarrays with isoenergetic pentamer and hexamer 2′-*O*-methyl oligonucleotide probes with LNA (locked nucleic acid) and 2,6-diaminopurine substitutions were used to probe the binding sites on the RNase P RNA specificity domain of *Bacillus subtilis*. Unexpected binding patterns were revealed. Because of their enhanced binding free energies, isoenergetic probes can break short duplexes, merge adjacent loops, and/or induce refolding. This suggests new approaches to the rational design of short oligonucleotide therapeutics but limits the utility of microarrays for providing constraints for RNA structure determination. The microarray results are compared to results from chemical mapping experiments, which do provide constraints. Results from both types of experiments indicate that the RNase P RNA folds similarly in 1 M Na^+ and 10 mM Mg^{2+}.

Binding of RNA to RNA is important for many natural functions, including protein synthesis (*1*, *2*), translation regulation (*3*, *4*), gene silencing (*5*, *6*), metabolic regulation (*7*), RNA modification (*8*, *9*), etc. (*10*−*13*). Binding of oligonucleotides to RNAs is important for therapeutic approaches, such as siRNA, ribozymes, and antisense therapy (*14*, *15*). Much remains to be discovered, however, of the rules for predicting binding sites and potential therapeutics.

Knowledge of RNA secondary and tertiary structures is useful for predicting binding sites for oligonucleotides (*16*−*18*). Definitive secondary structures of RNA can be determined by NMR[1] (*19*−*21*) and X-ray crystallography (*22*−*25*), but these methods are time-consuming and not applicable to every RNA. Most definitive RNA secondary structures were determined by comparative sequence analysis, which is based on the theory that homologous RNAs retain similar secondary structures during evolution even though their degree of sequence conservation is low (*26*, *27*). This method works well when a large number of homologous RNAs are available as inputs. Many novel RNAs, however, are being sequenced (*28*), and new RNA functions are often discovered without a large number of homologues. In these cases, structural mapping experiments using chemicals such as DMS, OH radicals, NMIA, etc., and/or ribonucleases provide a useful tool for secondary structure determination (*29*−*32*).

High-throughput microarray methods have also been developed to probe RNA structures (*33*−*38*). Thousands of oligonucleotide probes can be printed on a small glass chip. Binding of an RNA to the immobilized probes reveals all potential binding sites in a single experiment. Interpretation of the data is simplified by the use of isoenergetic probes, whose binding free energies are relatively sequence-independent (*37*, *38*). The probes are chimeras of 2′-*O*-methyl and locked nucleic acid (LNA) nucleotides with adenosine sometimes replaced with 2,6-diaminopurine (D). The modifications greatly enhance the binding free energies relative to DNA probes such that probes of five or six nucleotides with the sixth nucleotide being a 3′-terminal LNA guanosine provide sufficient binding strength (*39*, *40*). Thus, it is possible to interrogate all 1024 unique pentamer binding sites with a single microarray.

Here, we tested the isoenergetic microarray method combined with chemical mapping techniques on the secondary structure of the RNase P RNA specificity domain of *Bacillus subtilis* (RNRspBs). RNase P RNA exists in almost all organisms and is responsible for maturation of tRNA (*41*−*43*). In bacteria, the specificity domain of RNase P RNA recognizes substrate precursor tRNA (*44*). The crystal structure of RNRspBs has been determined by Krasilnikov et al. (*22*). Mortimer et al. (*29*) studied the solution structure of RNRspBs with selective 2′-hydroxyl acylation analyzed by primer extension (SHAPE). The secondary structure in vivo was deduced by sequence comparison and confirmed by the crystal structure (*22*, *45*, *46*).

The crystal structure of RNRspBs reveals several unique features (Figure 1). Most importantly, there are numerous tertiary interactions. For example, the nucleotides in J11/12 and J12/11 are arranged in a rigid structure by a hydrogen bond network. This and other tertiary interactions give the RNA a compact three-dimensional structure. The crystal structure provides an opportunity to test the information available from microarray experiments on a highly organized RNA. Unexpected binding patterns are observed for oligonucleotides.

[†]This work was supported by National Institutes of Health (NIH) Grant GM22939 (D.H.T.) and Ministry of Science and Higher Education Grants N N301 3383 33 (E.K.) and PBZ-MNiSW-07/I/2007 (R.K.). R.K. is the recipient of a Foundation for Polish Science fellowship.

*To whom correspondence should be addressed. Telephone: (585) 275-3207. Fax: (585) 276-0205. E-mail: turner@chem.rochester.edu.

[1]Abbreviations: CMCT, 1-cyclohexyl-3-(2-morpholinoethyl)carbodiimide metho-*p*-toluenesulfonate; D, 2,6-diaminopurine; DMS, dimethyl sulfate; HEPES, 4-(2-hydroxyethyl)-1-piperazineethanesulfonic acid; HPLC, high-performance liquid chromatography; LC−MS, liquid chromatography−mass spectrometry; LNA, locked nucleic acid; NMIA, *N*-methylisatoic anhydride; NMR, nuclear magnetic resonance; PAGE, polyacrylamide gel electrophoresis; RNRspBs, RNase P RNA specificity domain of *Bacillus subtilis*; SHAPE, selective 2′-hydroxyl acylation analyzed by primer extension; TLC, thin layer chromatography.

Published on Web 06/17/2010

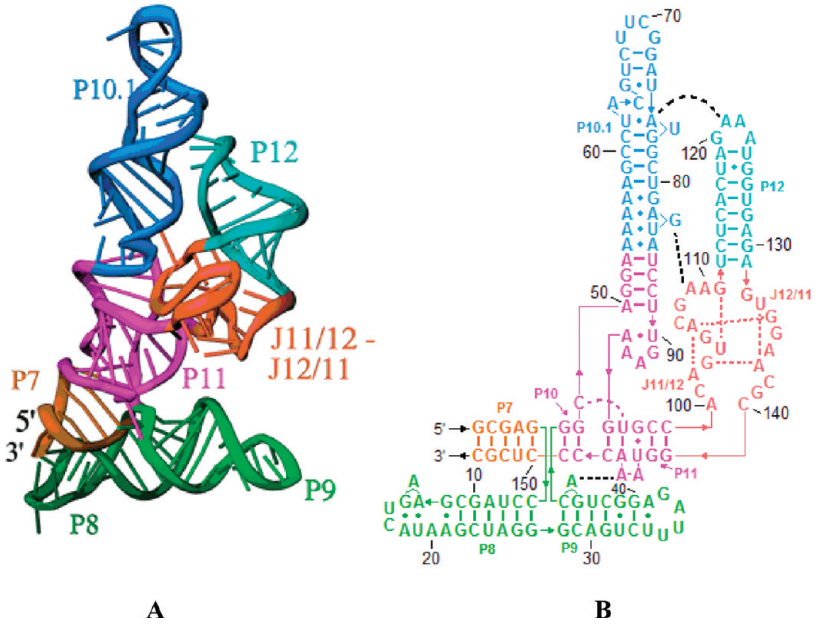

FIGURE 1: RNase P RNA specificity domain of *B. subtilis* (RNRspBs): tertiary structure (A) and secondary structure (B). Dashed lines in the secondary structure indicate observed tertiary interactions between connected nucleotides. Reprinted with permission from ref *22*. Copyright 2003 Macmillan Publishers Ltd.

MATERIALS AND METHODS

Materials. Plasmids carrying the gene for RNRspBs were kindly provided by A. Mondragón (*22*). Other materials and their sources are listed in the Supporting Information.

Chemical Synthesis of DNA, RNA, and 2′-O-Methyl Oligonucleotides. Isoenergetic oligonucleotide probes (pentamers and hexamers) with a 5′-end C6 amino linker were synthesized as described previously (*39*, *40*). DNA, RNA, and 2′-*O*-methyl oligonucleotides were synthesized on an Applied Biosystems 392 DNA/RNA synthesizer following the standard phosphoramidite approach (*47*, *48*). Deprotection and purification of oligonucleotides were performed according to the previously described procedure (*36*).

Molecular weights of oligonucleotides were checked by LC−MS (Hewlett-Packard 1100 MSD) with electrospray ionization. Purities were greater than 90% as determined with a Hewlett-Packard 1100 HPLC Chemstation with an analytical C18 reverse phase column. Concentrations were determined by UV absorption at 260 nm for DNA oligonucleotides and at 280 nm for RNA and 2′-*O*-methyl oligonucleotides.

Preparation of the B. subtilis RNase P RNA Specificity Domain. The plasmid carrying the RNRspBs gene was transfected into competent TOP10F′ *Escherichia coli* cells using the heat shock method in the presence of $CaCl_2$, and the transformed cells were stored in 20% glycerol stocks at −80 °C. Transformed *E. coli* cells from the stock were streaked on a Petri dish and grown overnight until colonies were ~1 mm in diameter. A single colony was picked and used to inoculate 5 mL of LB-ampicillin medium. The 5 mL culture was grown overnight to apparent turbidity and used to inoculate 2 L of LB-ampicillin medium, which was grown overnight with shaking at 250 rpm. Cells were collected and lysed, and the DNA plasmid was purified according to the standard protocol (*49*).

The plasmid was linearized by incubation at 37 °C for 1.5 h with the *Fok*I restriction enzyme. Completion of *Fok*I digestion was checked by agarose gel electrophoresis. The linearized plasmid was used as a template for in vitro transcription with T7 RNA polymerase at 42 °C for 1 h. RNA transcripts were purified by electrophoresis on a denaturing 6% polyacrylamide gel. The gel was visualized against a green fluorescent TLC plate under a hand-held UV light. The full-length RNA gel band was cut out with a flamed razor blade, and the RNA was electroeluted in 0.5× TA [1× TA being 40 mM Tris-acetate (pH 8.3)] buffer at 4 °C and 200 V for 2 h. Then, the RNA was ethanol precipitated, dried, redissolved in H_2O, and quantified by UV absorption at 260 nm assuming 1 OD_{260} = 40 μg/mL RNA.

Native Polyacrylamide Gel Electrophoresis (*PAGE*). RNRspBs samples were annealed in separate buffers containing various concentrations of metal ions. Folded RNRspBs samples were separated on a native 8% polyacrylamide gel cast in 1× TA buffer and run at 3 W and 4 °C for 8 h. After electrophoresis, the gel was rinsed briefly with H_2O and stained with SYBR Green II at 4 °C for 30 min with gentle shaking. The fluorescent image of the gel was scanned and recorded with a Molecular Dynamics Storm 840 Phosphorimager with a blue laser.

Folding RNA in Different Buffers. Buffers containing 40 mM HEPES, 40 mM NaHEPES, 100 mM NaCl, and *x* mM $MgCl_2$ (pH 8.0) are denoted by 140Na/80HEPES/*x*Mg. Buffers containing 25 mM HEPES, 25 mM NaHEPES, 135 mM KCl, and *x* mM $MgCl_2$ (pH 8.0) are denoted by 135K/25Na/50HEPES/*x*Mg. Buffers containing 25 mM HEPES, 25 mM NaHEPES, 135 mM KCl, and *x* M NaCl (pH 8.0) are denoted by 135K/25Na/50HEPES/*x*MNa.

For annealing, RNRspBs was first dissolved in buffers without $MgCl_2$. The RNA sample was incubated at 90 °C for 3 min and slowly cooled to 37 °C. At 37 °C, $MgCl_2$ was added to the desired concentration and the sample was incubated at 37 °C for 15 min. Then the sample was maintained at 37 °C or slowly cooled to 22 °C (room temperature) or 4 °C as desired for the experiments and further incubated for 20 min.

Labeling of RNRspBs, DNA Primers, and RNA Oligonucleotides. RNRspBs produced by T7 runoff transcription was dephosphorylated with shrimp alkaline phosphatase and purified on a denaturing 6% polyacrylamide gel before radiolabeling.

Dephosphorylated RNRspBs, chemically synthesized DNA primers, and RNA oligonucleotides were labeled with ^{32}P by incubation with [γ-^{32}P]ATP and T4 polynucleotide kinase at 37 °C for 1 h. After being labeled, the mixture was extracted with a phenol/chloroform mixture once and chloroform once followed by ethanol precipitation. The products were purified by running a denaturing 6% polyacrylamide gel. Product bands were imaged with X-ray films and cut out. RNRspBs was recovered by electroelution in 0.5× TA buffer, while DNA primers and RNA oligonucleotides were recovered by the crush-and-soak method in H_2O. Finally, the nucleic acids were ethanol precipitated and redissolved in H_2O.

Chemical Mapping. For mapping with DMS, CMCT, and kethoxal, RNRspBs was annealed in 20 μL of a folding buffer as described above and was kept at 22 or 4 °C. One microliter of 400 mM DMS in ethanol, 1 μL of 400 mM CMCT in ethanol, or 1 μL of 300 mM kethoxal in ethanol was added to each 20 μL sample, and each reaction mixture was incubated at 22 °C for 30 min or 4 °C for 1 h. At the end of the modification reaction, each sample was brought to 50 μL with H_2O and passed through a Clontech Chroma Spin-30 column immediately to remove chemicals. The column was further eluted with 50 μL of H_2O twice to maximize the recovery of the modified RNA. The modified RNA was then ethanol precipitated, dried, and redissolved to a concentration of 4 pmol/μL in H_2O.

For mapping with NMIA, RNRspBs was annealed in 30 μL of buffer and cooled to 22 or 4 °C as described above. Then 1 μL of 300 mM NMIA in DMSO was added to each sample, and the reaction mixture was incubated at 22 °C for 3.5 h or 4 °C for 20 h. Samples were shaken occasionally to ensure an even distribution of NMIA in the solution because NMIA is only slightly soluble in H_2O and would precipitate at the bottom over time. Modification was stopped by passing samples through Chroma Spin-30 columns to remove NMIA. Then samples were ethanol precipitated, dried, and redissolved to a concentration of 4 pmol/μL in H_2O.

Primer Extension of Chemical Mapping Products. Chemically modified nucleotides were identified by primer extension. The DNA primer (5′GCGAGGGGTTTACCGC), complementary to nucleotides 139−154, was 5′-end labeled with ^{32}P and then hybridized to RNA by incubating the mixture at 90 °C for 2 min, followed by annealing at 65 °C for 6 min, and finally incubating at 35 °C for 20 min. Primer extension was initiated by addition of 1 μL AMV reverse transcriptase, and the 10 μL reaction mixture was incubated for 10 min at 37 °C. The extension reaction was stopped by addition of 1 μL of 4 M NaOH and heating at 95 °C for 5 min. The samples were ethanol precipitated and redissolved in Loading Buffer II from Ambion, containing formamide. Extended DNA products were separated with a denaturing 6% polyacrylamide gel, which was then dried on Whatman paper and exposed to a phosphor screen. The phosphor screen was scanned with a Bio-Rad Personal Molecular Imager, and the bands were identified by comparison to sequencing lanes and quantified relative to control lanes with ImageQuant version 5.2.

Isoenergetic Microarrays. A total of 116 isoenergetic pentamer and hexamer (with 3′-LNA G) probes were synthesized (see Table S1 of the Supporting Information) and printed in triplicate on microarrays along with mono-U and UUUUU as negative controls and a 25-mer DNA probe as a positive control. Spotting buffer was also printed on several spots as a negative control. Spots were arranged in 16 blocks of 3 × 10 spots at a spot distance of 450 μm, except the last four blocks which had one row of three spots. The blocks were spaced 1.95 mm apart in length and 3.60 mm apart in width.

Fabrication of isoenergetic microarrays was based on the method of Afanassiev et al. (*50*), with some changes. Aminoalkylsilane-treated glass slides were coated with 2% agarose activated with $NaIO_4$ at a level of 0.213 g/g of agarose. After the agarose solidified for 1 h, slides were washed with H_2O for 3 h, dried in air, and stored in the dark at room temperature. Probes at 200 μM in a spotting buffer (3× SSC (standard saline citrate, 1× SSC being 150 mM NaCl and 15 mM sodium citrate), 0.05% SDS (sodium dodecyl sulfate), 0.001% CHAPS {3-[(3-cholamidopropyl)dimethylammonio]-1-propanesulfonate}) were printed on the glass slides with a MicroGrid II TAS Arrayer at the Microarray and Genomics Facility, Roswell Park Cancer Institute, Buffalo, NY. Printed microarrays were incubated in a humid chamber at 37 °C for 12 h for the probes to bond with the agarose gel matrix. After incubation, microarrays were immersed in a freshly prepared 35 mM $NaBH_4$ solution in PBS buffer [137 mM NaCl, 2.7 mM KCl, 4.3 mM Na_2HPO_4, and 1.4 mM KH_2PO_4 (pH 7.5)] and ethanol (3:1, v/v) at room temperature for 15 min to reduce the uncoupled aldehyde groups. They were washed three times (30 min each) in H_2O at room temperature, then in 1% SDS at 55 °C for 1 h, and finally three times (30 min each) in H_2O at room temperature. Microarrays were dried at room temperature and stored in the dark.

Hybridization of RNRspBs on the Microarray. ^{32}P-labeled RNRspBs was annealed in appropriate buffers as described previously and cooled to 4 °C. Microarrays were presoaked with the same buffer at 4 °C for 30 min, and the soaking buffer was removed by a brief centrifugation of the slides in a clinical centrifuge. Immediately afterward, 180 μL of the annealed RNRspBs sample at 50 nM was dispensed on the surface of the microarray and the microarray was covered with a probe-clip press seal incubation chamber. Hybridization proceeded at 4 °C for 24 h in a humid chamber half-filled with H_2O to ensure 100% humidity. Subsequently, the probe-clip incubation chamber was removed and the solution was decanted. The hybridized microarray was centrifuged briefly in a clinical centrifuge to remove excess liquid. Then, it was washed with the same hybridization buffer at 0 °C twice, 30 s each, to remove unbound and nonspecifically bound RNRspBs and briefly centrifuged in a clinical centrifuge to remove excess liquid. The microarray was wrapped with a plastic membrane and exposed to a phosphor screen at room temperature. The screen was scanned and recorded with a Molecular Dynamics Storm 840 Phosphorimager. Binding intensities were quantified with ImageQuant version 5.2 and AGScan (AGScan Project, http://mulcyber.toulouse.inra.fr/projects/agscan).

Only when all three microarray spots corresponding to the same probe become darker simultaneously was the probe considered to bind to RNRspBs. The radioactivity of each spot was integrated over the pixels within the area of a fixed diameter. The radioactivity for each probe was calculated by averaging the intensities of the three spots of the probe. The background intensity was obtained for areas within circles of the same diameter in the vicinity of the spots and subtracted from the average intensity to generate the net intensity due to binding of the probe.

RNRspBs Probe Binding Site Footprinting. Probes 5′CU^{L}CG^{L}CG^L (probe 3) and 5′GC^{L}UD^{L}GG^L (probe 9), fully complementary to nucleotides 1−5 and 6−11, respectively, were hybridized with RNRspBs. RNRspBs bound with probe was

chemically modified with NMIA and kethoxal to identify the probe's binding sites.

Five nanomoles of probe was dissolved in 10 μL of 135K/25Na/50HEPES/10Mg buffer and added to 25 pmol of RNRspBs annealed in 30 μL of 135K/25Na/50HEPES/10Mg buffer. The final RNRspBs concentration was 0.625 μM, and the probe concentration was 125 μM. The probe was hybridized to RNRspBs for 24 h at 22 °C. Hybridized RNRspBs was modified at 22 °C by 10 mM NMIA for 4 h or by 15 mM kethoxal for 1 h. The reaction was quenched by two ethanol precipitations and a Clontech Chroma Spin-30 column filtration to remove probe and NMIA or kethoxal. The sites of increased or decreased NMIA and kethoxal modifications were read out by primer extension with a DNA primer, 5′TCACTGTGGCACTTTCAAGG, complementary to nucleotides 87−106, as described for chemical mapping.

RNase H Assay with Antisense Oligodeoxyribonucleotides. DNA oligonucleotides were synthesized: 5′GCTAGGCTCGC (GC1−11), 5′TCGCTAGGCTCGC (TC1−13), 5′ACTGCCCTAGCTT (AT20−32), 5′GAAGACGTAGGCTT (GT57−70), 5′ATACTCAGCCATAT (AT73−86), 5′CTTCGTCACTGTGGC (CC97−111), and 5′GCGTTCCACTC (GC130−140). Their naming in the parentheses, taking GC1−11 for example, provides information about the 5′- and 3′-nucleotides (GC) and the RNA region it complements (1−11).

Twenty picomoles of RNRspBs was annealed as described previously in 20 μL of 135K/25Na/50HEPES/10Mg buffer. Individual DNA oligonucleotides at 20 nmol each in 20 μL of 135K/25Na/50HEPES/10Mg buffer were added to annealed RNRspBs, and the hybridization mixture was incubated for 24 h at 22 °C. Then, 10 units of RNase H was added, and the samples were incubated for 4 h at 22 °C. Reactions were stopped by acid phenol/chloroform (pH 4.5) extraction that removed both RNase H enzyme and antisense DNA oligonucleotides. The samples were precipitated with 100% ethanol, washed with 80% ethanol, and redissolved in H_2O. Cleavage sites were read out by primer extension as described for chemical mapping.

Calculations of Binding Free Energies. Binding free energies of probes that bind strongly to the RNA at the predicted binding sites and potential alternative binding sites were calculated at 4, 22, and 37 °C using the nearest neighbor model and 2′-*O*-methyl RNA/RNA parameters with bonuses for LNA modifications (*37*−*40*). If probes are complementary to base-paired nucleotides, then they may bind by causing the RNA to rearrange its structure. In that case, only local structural rearrangements were considered. For probe binding to the folded RNA in solution, bimolecular folding of probe was considered while unimolecular folding of the probe was ignored due to the short length of the probes. When binding occurs on the surface of the microarray, however, the probes are immobilized on the microarray surface and unlikely to associate bimolecularly. Therefore, only the unimolecular folding of the RNA and the bimolecular folding of the probe with the RNA were considered.

RESULTS

Structural Response of RNRspBs to Different Ionic Conditions Revealed by Native PAGE. The compact structure of RNRspBs is stabilized by extensive tertiary interactions (*22*) that are dependent on salt conditions (*29*). The effects of varying concentrations of monovalent and divalent metal ions on RNRspBs structure were qualitatively studied by the mobility and sharpness of RNA bands in native PAGE (Figure S1 of the Supporting Information). The sharpest bands are observed at ≥5 mM Mg^{2+}. The RNA always migrates as a single band, but the sharpness of the band indicates the degree of rigidity of the tertiary structure. Evidently, the tertiary interactions are completely formed to give the RNA a single compact folding when the Mg^{2+} concentration is above 5 mM. Sharp bands are also observed when buffers contain 1 M NaCl or 500 mM KCl in the absence of Mg^{2+}.

Chemical Mapping of RNRspBs. RNRspBs was crystallized at 5 mM $MgCl_2$ (pH 6.0) without Na^+ or K^+ (*22*). Chemical mapping with 1-methyl-7-nitroisatoic anhydride (1M7) in 100 mM NaCl and 6 mM $MgCl_2$ (pH 8.0) to identify conformationally flexible and solvent accessible ribose rings gave results consistent with the crystal structure (*29*). To test the structure of RNRspBs and its reactivity to other chemicals under different conditions, we chemically mapped it with DMS, CMCT, kethoxal, and NMIA at both 4 and 22 °C. DMS modifies N1 atoms of adenosines and N3 atoms of cytidines; CMCT modifies N3 atoms of uridines and to a lesser extent N1 atoms of guanosines (*31*), and kethoxal modifies N1 and N2 atoms of guanosines (*32*). 140Na/80HEPES/10Mg, 135K/25Na/50HEPES/10Mg, 135K/25Na/50HEPES/0Mg, and 135K/25Na/50HEPES/1MNa buffers were used. The modifications are very similar at both temperatures, indicating that RNRspBs folding is independent of temperature between 4 and 22 °C. The modifications are also similar in 140Na/80HEPES/10Mg, 135K/25Na/50HEPES/10Mg, and 135K/25Na/50HEPES/1MNa (Figure 2). The similarity of results when 10 mM Mg^{2+} is replaced with 1 M Na^+ indicates that 1 M Na^+ stabilizes the tertiary structure, consistent with the native PAGE experiment. Many more modifications are observed in 135K/25Na/50HEPES/0Mg, however, particularly for nucleotides 89−96, for J11/12 and J12/11, and for the GAAA tetraloop (Figure 2). This has also been seen with 1M7 (*29*) and is expected if Mg^{2+} stabilizes tertiary interactions (*52*−*54*).

Chemical mapping in all the buffers is consistent with the secondary structure determined by X-ray crystallography (Figure 2). Reactive nucleotides are mostly in the hairpin loops of P8, P9, and P10.1 and in the lower internal loop in P10.1. In 135K/25Na/50HEPES/0Mg buffer, nucleotides in J11/12 and J12/11 and hairpin loop GAAA in P12 become strongly reactive (Figure 2C). In the presence of 10 mM Mg^{2+}, J11/12 and J12/11 have a complex hydrogen bonding and stacking network that largely protects these nucleotides from being modified by chemicals. Evidently, this structure is not stable when the only cations are 135 mM K^+ and 25 mM Na^+. Similarly, the GAAA hairpin loop forms tertiary interactions with the tetraloop receptor region (top internal loop) in P10.1 and is also not accessible when Mg^{2+} is present (Figure 2A,B). These tertiary interactions are also apparently not stable in 135 mM K^+, 25 mM Na^+, and 0 mM Mg^{2+} (Figure 2C). Another difference between 135K/25Na/50HEPES/10Mg and 135K/25Na/50HEPES/0Mg buffers is that nucleotides 89−95 are strongly modified in 135K/25Na/50HEPES/0Mg buffer (inset of Figure 2C), but protected in the presence of 10 mM Mg^{2+}. These nucleotides are buried at the center of the RNA in the crystal structure (*22*). Evidently, this shields the nucleotides from chemical modification when Mg^{2+} stabilizes the tertiary structure. When Mg^{2+} is replaced with 1 M Na^+, more nucleotides in J11/12 and J12/11 are modified but not as strongly as in the buffer containing only 135 mM K^+, 25 mM Na^+, and 0 mM Mg^{2+} (Figure 2D). This indicates that 1 M Na^+ can partially restore the tertiary interactions disrupted due to the absence of Mg^{2+}.

Modeling RNRspBs Secondary Structure. RNRspBs has a complex three-dimensional structure and thus provides a stringent test of methods for modeling secondary structure. When no

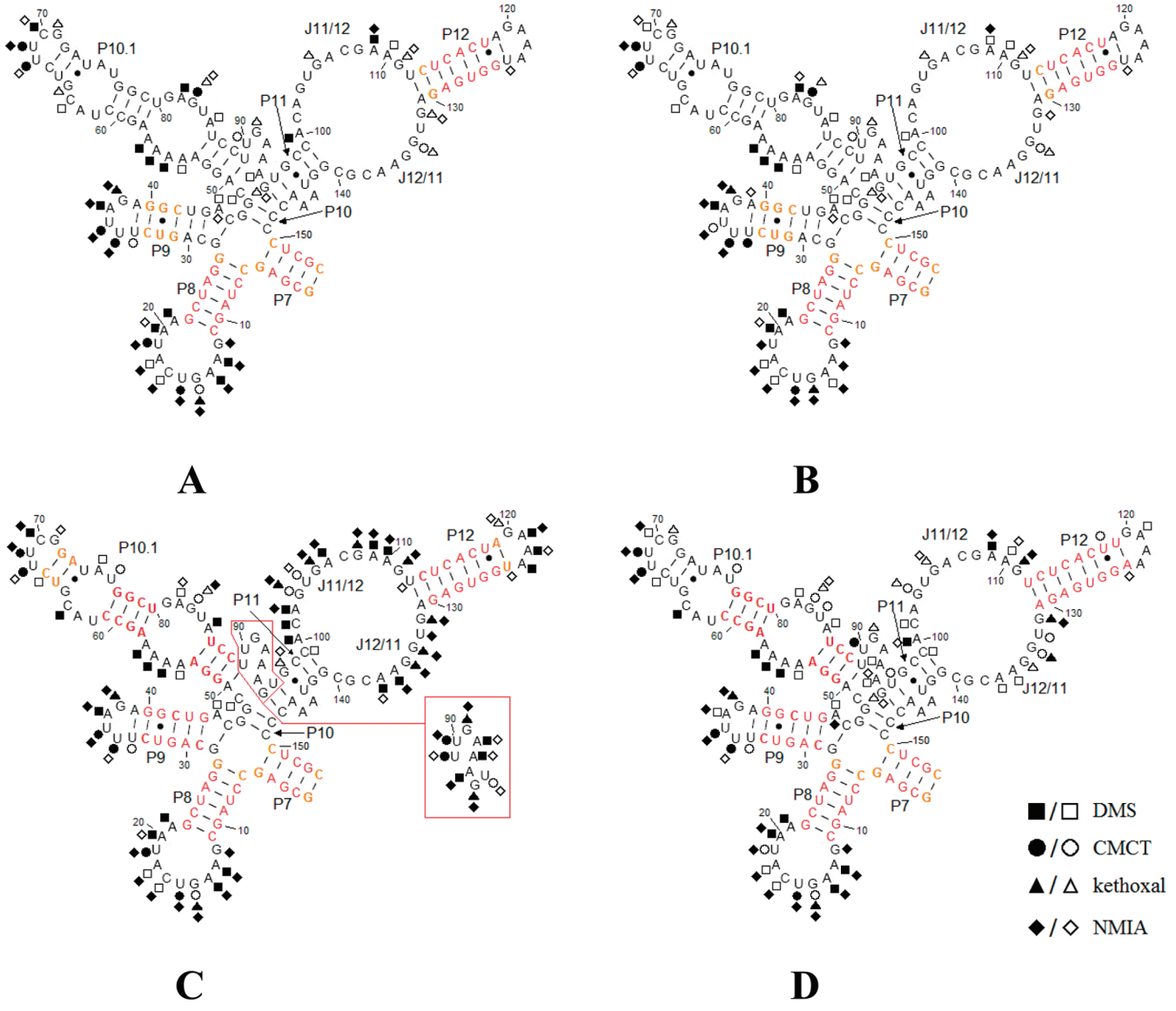

FIGURE 2: Chemical modifications of RNRspBs at 22 °C by DMS (■), CMCT (●), kethoxal (▲), and NMIA (◆) in (A) 135K/25Na/50HEPES/10Mg, (B) 140Na/80HEPES/10Mg, (C) 135K/25Na/50HEPES/0Mg, and (D) 135K/25Na/50HEPES/1MNa. Filled symbols indicate strong modifications. Empty symbols indicate moderate modifications. Base pairs colored orange and red are predicted by RNAstructure 4.6 constrained by strong plus medium reactivity in mapping data to have >95 and >99% base pair probability, respectively.

constraints are applied, RNAstructure 4.6 with "Window Size" set at 0 and "Temperature" set at 310.15 K predicts a minimum free energy (MFE) structure that has 79.5% of known canonical base pairs (Table 1) and a folding ΔG°_{37} of −49.9 kcal/mol calculated with Energy Function 2 (EFN2) (Figure 3, left structure), which calculates the free energy with more rules than used in the dynamic programming algorithm (*51*). The 20 structures with the lowest free energies have an average of 68.4% accurately predicted base pairs. The best predicted structure has a 93.2% accuracy, is predicted to fold at −47.6 kcal/mol, and is ranked 22nd by ΔG°_{37} (Figure 3, right structure). Compared to the correct structure, whose predicted free energy is −41.6 kcal/mol, the best predicted structure is different only in three places: (1) the formation of 4 bp (G103-C138, U104-A137, C107-G134, and G108-U133) between J11/12 and J12/11, (2) the missing G28-C46 base pair between the A45 bulge and the four-way multibranch loop, and (3) the slipping of the C147-C148-C149 sequence that results in slipping the U96-A146 base pair to U96-A144, slipping of the A144-A145 bulge loop to the A145-A146 bulge loop, and leaving C149 unpaired. The misprediction by the RNAstructure algorithm is the result of its inability to consider stabilizing tertiary interactions that can have subtle effects on secondary structure. A partition function calculation (*55*) shows that nucleotides in P7, P8, and P12 have a >99% probability of forming base pairs and nucleotides in P9 have a >95% probability of forming base pairs (Figure 3). Base pairs in other predicted duplexes have lower certainties and are indeed prone to misprediction. All base pairs predicted with >95% probability are present in the known structure and comprise 45.5% of the known base pairs.

The RNAstructure algorithm can constrain reactive nucleotides not to be in a Watson−Crick base pair flanked on each side by a Watson−Crick base pair. When the strong and intermediate chemical modifications are used as constraints in RNAstructure 4.6, the MFE secondary structure still has 79.5% of known base pairs but the structure with 93.2% correctly predicted Watson−Crick base pairs is now ranked between sixth and eighth, and the most accurate structure is improved to have 95.5 or 97.7%

Table 1: RNRspBs Secondary Structure Prediction Accuracy by RNAstructure 4.6 with and without Strong and Intermediate Chemical Mapping Constraints in Different Buffers[a]

		experimental constraints from chemical mapping with DMS, CMCT, kethoxal, and NMIA								
		135K/25Na/50HEPES/10Mg (140Na/80HEPES/10Mg)			135K/25Na/50HEPES/0Mg			135K/25Na/50HEPES/1MNa		
		no. of constraints			no. of constraints			no. of constraints		
	no experimental constraints	DMS, CMCT, and kethoxal	NMIA	total no. of unique constraints[b]	DMS, CMCT, and kethoxal	NMIA	total no. of unique constraints[b]	DMS, CMCT, and kethoxal	NMIA	total no. of unique constraints[b]
no. of constraints	not applicable	40 (36)	23 (24)	42 (42)	60	48	65	52	27	54
minimum ΔG°_{37} structure	79.5%		79.5%			79.5%			79.5%	
average of 20 lowest-ΔG°_{37} structures	68.4%		81.4%			82.4%			82.2%	
best predicted structure (rank)	93.2% (22nd)		97.7% (30th)			95.5% (35th)			95.5% (39th)	
rank of 93.2% accurate structure	22nd		8th			6th			7th	

[a]To be counted as accurate, a base pair had to be identical to a base pair in the crystal structure (*22*). [b]The total number of unique constraints is the number of nucleotides modified by one or more reagents so that overlaps are not counted.

correct Watson−Crick base pairs (Table 1). The average accuracy of the 20 structures with the lowest free energies is improved and is between 81.4 and 82.4%.

The misprediction in the MFE structure occurs in P10, the base of P10.1, and P11, which close multibranch loops (Figure 3). Helix, 5′G47G48C49A50/3′C99C98G97U96, is formed, forcing nucleotides U89−G95 to form a bulge loop and nucleotides G141−C148 to form a hairpin loop (Figure 3). Constraints from chemical mapping work well in RNAs consisting of long duplexes. In RNRspBs, however, the initial helix of P10 has 2 bp and P11 contains a G97-U143 wobble pair next to an A144-A145 bulge loop. Therefore, the constraints are not enough for RNAstructure to determine which nucleotides are base-paired and which nucleotides are single-stranded in the prediction of the MFE structure.

Isoenergetic Oligonucleotide Microarray. RNRspBs has 150 pentamer binding sites. Isoenergetic pentamer and hexamer probes that are Watson−Crick complementary to 127 of the sites were printed on microarrays. The other 23 positions have long A and U stretches for which no probes can be designed with the required binding free energies. The pentamer probes are identified by the position of the nucleotide in RNRspBs that binds to the middle nucleotide of the probe. Hexamer probes are identified as pentamers ignoring the 3′-terminal LNA G. There are 19 pentamer and 97 hexamer probes (Table S1 of the Supporting Information). Eleven probes each have two fully complementary pentamer sites.

The isoenergetic probes' binding free energies for binding to complementary unstructured RNA are much more favorable than those of both 6-mer DNA probes and 2′-*O*-methyl probes without LNA or 2,6-diaminopurine modifications. They are also roughly sequence-independent compared to 6-mer DNA probes (Figure S2 of the Supporting Information). At 37 °C and 100 mM NaCl, the isoenergetic probes specific for RNRspBs have predicted binding free energies ranging from −7.9 to −12.7 kcal/mol, with most between −8.0 and −11.0 kcal/mol. Six hexamer probes bind to the unstructured target with a free energy more favorable than −12.0 kcal/mol because the 3′-LNA G's form G^L-C pairs with the RNA. The LNA G at the 3′-end of the hexamer probes increases stability by approximately 1.5 kcal/mol when it forms G^L-A, G^L-G, or G^L-U mismatches with the target and by ∼3.5 kcal/mol when it forms G^L-C pairs (*56*). The average of predicted binding free energies of the isoenergetic probes used in the study is -10.0 ± 1.0 kcal/mol in 100 mM NaCl at 37 °C. For comparison, the 2′-*O*-methyl probes of the same sequences without any modifications average -6.1 ± 0.9 kcal/mol and range between −3.6 and −8.9 kcal/mol. Hexamer DNA probes calculated from OligoWalk (*57*) range from −0.3 to −8.1 kcal/mol with an average of -4.5 ± 1.6 kcal/mol at 37 °C and 1 M NaCl (Figure S2 of the Supporting Information). The greater stability of duplexes formed between isoenergetic probes and RNA allows the use of short probes in microarray experiments. Table S1 of the Supporting Information contains complete information about probes, including predicted ΔG°_{37} values for binding to unstructured RNA.

RNRspBs Binding to Oligonucleotides on Isoenergetic Microarrays. Binding of RNRspBs to isoenergetic microarrays at 4 °C was assessed in 140Na/80HEPES/10Mg, 135K/25Na/50HEPES/10Mg, and 135K/25Na/50HEPES/1MNa (Figure 4). For all three buffer conditions, probe 17 binds strongly to the hairpin loop closed by P8. As shown in Figure 5, the intensities of spots were normalized to the intensity for probe 17 to compare

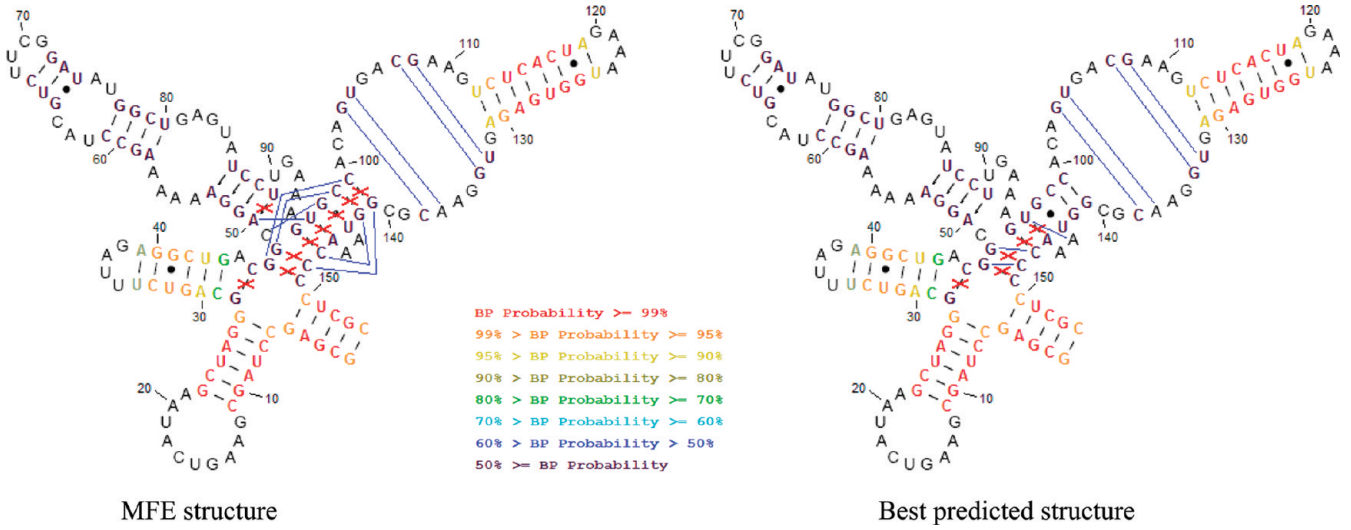

FIGURE 3: RNRspBs structural prediction by RNAstructure 4.6 without experimental constraints. The minimum free energy (MFE) structure has the lowest free energy calculated by EFN2 (left), and the best predicted structure has the most accurately predicted Watson−Crick pairs (right). Red X's indicate missing base pairs. Blue lines indicate incorrect base pairs. The color code indicates the base pair probability calculated by partition function (*55*).

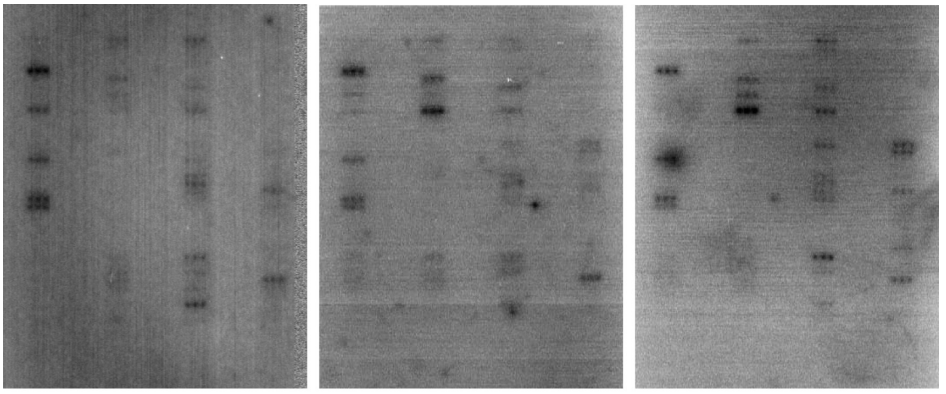

FIGURE 4: Results of hybridization of RNRspBs to isoenergetic microarrays in three different buffers at 4 °C: (A) 140Na/80HEPES/10Mg, (B) 135K/25Na/50HEPES/10Mg, and (C) 135K/25Na/50HEPES/1MNa.

binding under different buffer conditions:

$$\text{normalized intensity} = \frac{\text{average intensity of three spots} - \text{background intensity}}{(\text{average intensity of three spots} - \text{background intensity})_{\text{probe17}}}$$

Probes with normalized intensities that are more than one-third of the maximum normalized intensity are considered strong binding. Probes with normalized intensities between one-third and one-ninth of the maximum normalized intensity are considered intermediate binding. Probes with normalized intensities that are less than one-ninth of the maximum normalized intensity are considered weak or no binding. Qualitative results are summarized in Table 2.

Comparisons of binding in 140Na/80HEPES/10Mg and 135K/25Na/50HEPES/1MNa buffers to that in 135K/25Na/50HEPES/10Mg buffer are made by taking the differences of their normalized intensities according to

$$\text{relative intensity} = \text{normalized intensity}_{\text{buffer X}} - \text{normalized intensity}_{\text{135K/25Na/50HEPES/10Mg}}$$

Buffer X denotes 140Na/80HEPES/10Mg or 135K/25Na/50HEPES/1MNa. The relative intensities are plotted in Figure 6.

The binding sites for many probes are ambiguous either because two sites have identical sequences or the predicted $\Delta G°$ for a probe binding an alternative site with a mismatch is more favorable than −8 kcal/mol and RNRspBs binds moderately or strongly to the probe with perfect complementarity to the site. In Table 2, probes targeting two sites with identical sequences have the second site listed in parentheses. Alternative sites that could bind a given probe are listed in brackets. Figure 7 provides a summary of probe binding.

The strongest or second strongest binding is seen for probe 17, which targets the largest hairpin loop. Two of the three other hairpin loops also bind to probes. The exception is the GAAA tetraloop capping P12. This tetraloop is also the hairpin loop least reactive to small chemicals in the presence of 10 mM Mg^{2+} (Figure 2).

Several helical regions unexpectedly bind probes. These include P7, P8, the base helix of P10.1, and P12. Probes are apparently able to invade intramolecular helices that abut multibranch or large internal loops.

Strong and intermediate binding sites in 135K/25Na/50HEPES/1MNa are similar to those in the buffers containing 10 mM Mg^{2+}, although the intensity of bound radioactivity is often stronger

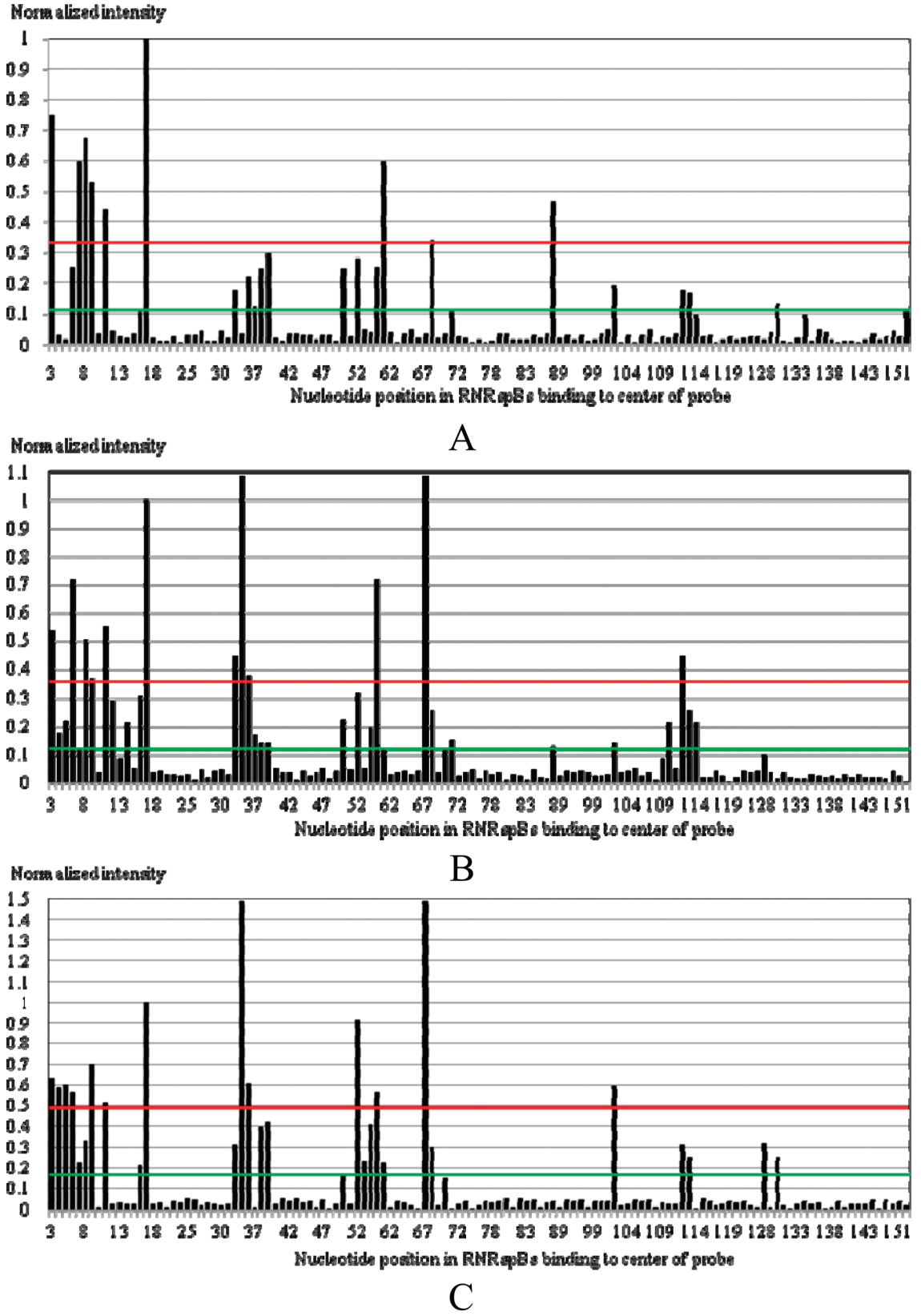

FIGURE 5: Quantification of microarray hybridization results. RNRspBs was folded in (A) 140Na/80HEPES/10Mg, (B) 135K/25Na/50HEPES/10Mg, and (C) 135K/25Na/50HEPES/1MNa buffers and hybridized to an isoenergetic microarray at 4 °C for 24 h. Probe binding strength is represented by normalized intensity: normalized intensity = (average intensity − background intensity)/(average intensity − background intensity)$_{probe\ 17}$, where average intensity is the average of three spots of the same probe. Probes with normalized intensities that are more than one-third of the maximum normalized intensity (red line) are strong binding. Probes with normalized intensities between one-third and one-ninth of the maximum normalized intensity (green line) are intermediate binding. Probes with normalized intensities that are less than one-ninth of the maximum normalized intensity are weak or no binding.

in 1 M Na^+ (Table 2 and Figures 4−7). The results suggest that 1 M Na^+ supports tertiary interactions to some extent, which is consistent with the results from native PAGE and chemical mapping.

Table 2: Binding Strengths of Isoenergetic Probes in 140Na/80HEPES/10Mg, 135K/25Na/50HEPES/10Mg, and 135K/25Na/50HEPES/1MNa Buffers at 4 °C[a]

nucleotide position in target RNA binding to middle of probe[b]	sequence of probe[c]	$\Delta G°_{37}$ (probe/RNA, 0.1 M NaCl) (kcal/mol)[d]	binding strength[e] 140Na/80HEPES/10Mg	135K/25Na/50HEPES/10Mg	135K/25Na/50HEPES/1MNa
3	$CU^LCG^LCG^L$	−10.3	s	s	s
4	$G^LCU^LCG^L$	−9.1	w	m	s
5	GGC^LUC^L	−9.4	w	m	s
6 (60) [32]	$AG^LGC^LUG^L$	−10.6 [−10.3]	m	s	s
7 (61)	$UD^LGG^LCG^L$	−10.5	s	w	m
8	$CUD^LGG^LG^L$	−10.5	s	s	m
9	$GC^LUD^LGG^L$	−12.7	s	s	s
11	$UC^LGC^LUG^L$	−10.2	s	s	s
12 [140]	$U^LUC^LGC^LG^L$	−10.3 [−11.2]	w	m	w
14 (110)	$DC^LUU^LCG^L$	−10.0	w	m	w
16	$U^LGD^LCU^LG^L$	−8.9	w	m	m
17	$D^LUG^LDC^LG^L$	−10.4	s	s	s
32 (112)	$D^LGD^LCU^LG^L$	−11.7	m	s	m
33 (67)	$D^LDG^LDC^LG^L$	−10.5	w	s	s
34	$D^LDD^LGA^LG^L$	−9.3	m	s	s
37	$U^LCU^LDD^LG^L$	−9.0	m	m	w
38	$C^LUC^LUD^LG^L$	−10.2	m	m	m
39	$CC^LUC^LUG^L$	−10.1	m	m	m
50	CC^LUG^LC	−9.7	m	m	w
52	$U^LUC^LCU^LG^L$	−10.8	m	m	s
53	$U^LUU^LCC^LG^L$	−8.4	w	w	m
59 [4] [5]	$G^LGC^LUU^LG^L$	−10.0 [−12.2]	w	m	m
60 (6) [32]	$AG^LGC^LUG^L$	−10.6 [−10.3]	m	s	s
61 (7)	$UD^LGG^LCG^L$	−10.5	s	w	m
67 (33)	$D^LDG^LDC^LG^L$	−12.0	w	s	s
68 [34]	$GD^LDG^LDG^L$	−9.7 [−8.0]	s	m	m
71	$UC^LCG^LDG^L$	−10.5	w	m	w
88 [34]	$D^LDG^LGD^LG^L$	−11.5 [−9.4]	s	m	w
102 [140] [141]	$DC^LUG^LUG^L$	−11.1 [−11.4]	m	m	s
110 (14)	$DC^LUU^LCG^L$	−10.0	w	m	w
112 (32)	$D^LGD^LCU^LG^L$	−9.5	m	s	m
113 [33] [66] [67]	$GD^LGD^LCG^L$	−9.8 [−8.1] [−10.2]	m	m	m
114	$U^LGD^LGD^LG^L$	−11.0	w	m	w
128	$CUC^LDC^LG^L$	−9.8	w	w	m
130	$CUC^LUC^LG^L$	−10.0	m	w	m
152	GC^LGD^LG	−9.6	m	w	w

[a]Probes that bind to RNRspBs weakly in all three buffers are not listed. Probes corresponding to nucleotide positions 19, 20, 35, 36, 54−58, 75, 84, 91−95, 120−123, and 144−146 in RNA were not used because no modifications can provide sufficient binding free energies. [b]Pentamer probes are identified by the position of the nucleotide in RNRspBs that binds to the center nucleotide of the probe. Hexamer probes are identified as pentamer probes ignoring the 3′-LNA G. Alternative fully complementary sites are listed in parentheses. Potential alternative binding sites are listed in brackets. [c]Probes are 2′-*O*-methyl and LNA chimera oligonucleotides. LNA nucleotides are designated by a superscript L. [d]Values indicate the predicted $\Delta G°_{37}$ values of probes binding to their unfolded complementary sites. The $\Delta G°_{37}$ values of probes binding to their potential alternative binding sites are listed in brackets corresponding to the first column. Only one $\Delta G°_{37}$ value is given for two adjacent potential alternative binding sites of a probe. Calculation considers only the formation of 5 bp formed between the probe and its binding site in RNRspBs and the base pair (−3 kcal/mol) or mismatch (−1.5 kcal/mol) formed between the 3′-terminal LNA G of the probe and C or A, G, and U of RNRspBs in some cases (56) but does not consider the 3′- or 5′-dangling ends from RNRspBs. [e]s indicates strong binding (normalized binding intensity that is at least one-third of the maximum normalized intensity). m indicates intermediate binding (one-third of the maximum normalized intensity > normalized binding intensity ≥ one-ninth of the maximum normalized intensity). w indicates weak or no binding (normalized binding intensity < one-ninth of the normalized intensity). Normalized binding intensity is calculated by the equation normalized intensity = (average intensity of three spots − background intensity)/(average intensity of three spots − background intensity)$_{\text{probe 17}}$, where both spot and background intensities are directly measured from the radioactivity on the microarray.

Hybridizations in other buffers and at other temperatures were also performed. These include 140Na/80HEPES/5Mg and 140Na/80HEPES/0Mg at 4 °C, 135K/25Na/50HEPES/10Mg at 22 °C, and 140Na/80HEPES/10Mg at 37 °C (data not shown). The binding intensities of probes depend on the hybridization conditions and are reduced to various degrees. Only a few probes remain strongly bound and give apparent signals. For example, probes 11 and 17 remain strongly bound in 140Na/80HEPES/5Mg, while the binding intensities of other probes are reduced compared to that in 140Na/80HEPES/10Mg at 4 °C. In 140Na/80HEPES/0Mg, only probe 17 still binds strongly at 4 °C. In 140Na/80HEPES/10Mg buffer at 37 °C, only probes 9 and 17 show binding signals, albeit very weak. When the microarray experiment was conducted in 135K/25Na/50HEPES/10Mg at 22 °C, only probe 17 remains strongly bound and probes 9, 32(112), and 33(67) show weak to intermediate binding signals.

Footprinting of Probe 3 and 9 Binding Sites on RNRspBs. The chemical mapping results confirmed that the RNRspBs secondary structure in solution is consistent with that determined from the crystal structure (*22*), from sequence comparison (*45*, *46*), and from 1M7 chemical mapping under somewhat different conditions (*29*). Comparison of the secondary structure with the microarray results led to the hypothesis that binding of probes on the microarray surface may induce structural rearrangement

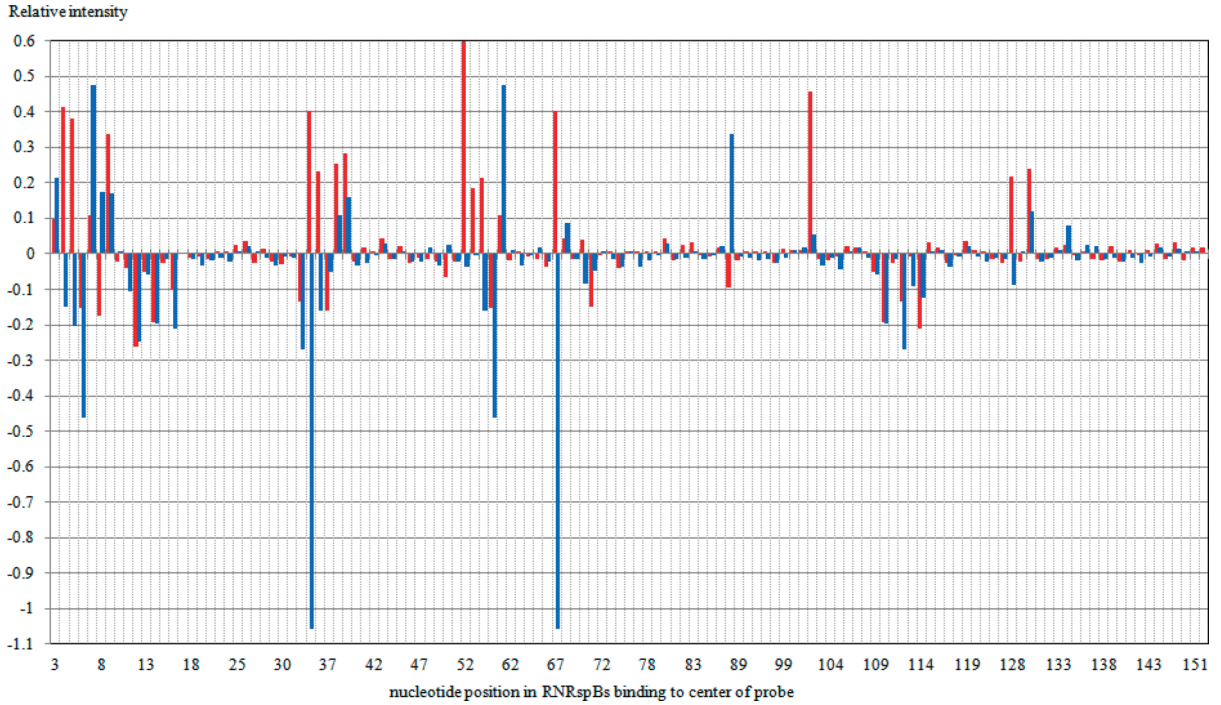

FIGURE 6: Relative intensities of RNRspBs binding to probes under different salt conditions. Blue bars indicate relative intensities of probes in 140Na/80HEPES/10Mg and 135K/25Na/50HEPES/10Mg. Red bars indicate relative intensities of probes in 135K/25Na/50HEPES/1MNa and 135K/25Na/50HEPES/10Mg. Relative intensities are calculated with the equation, relative intensity = normalized intensity$_{\text{buffer X}}$ − normalized intensity$_{\text{135K/25Na/50HEPES/10Mg}}$. Buffer X denotes 140Na/80HEPES/10Mg or 135K/25Na/50HEPES/1MNa. Positive values indicate that probes bind more tightly in 140Na/80HEPES/10Mg or in 135K/25Na/50HEPES/1MNa buffer than in 135K/25Na/50HEPES/10Mg buffer. Negative values indicate that probes bind more tightly in 135K/25Na/50HEPES/10Mg buffer than in either 140Na/80HEPES/10Mg or 135K/25Na/50HEPES/1MNa buffer.

of RNRspBs. To test that hypothesis, binding of probes 3 and 9 was footprinted in solution separately with NMIA and kethoxal (Figure S3 of the Supporting Information).

In the presence of probe 3, an increased degree of NMIA modification is observed at U8, G10, and C11 (Figure S3A, lane 2 vs lane 1) and an increased degree of kethoxal modification at G9 (Figure S3B, lane 3 vs lane 1). This is consistent with probe 3, 5′CU^{L}CG^{L}CG^{L}, binding to nucleotides 1−5 and causing the nucleotides at the 3′-terminus of the RNA to pair with nucleotides 22−27, leaving nucleotides 6−11 open for NMIA or kethoxal modification. In the presence of probe 9, 5′GC^{L}UD^{L}GG^{L}, an increased degree of NMIA modification is observed for nucleotides 25−28 (Figure S3A, lane 3 vs lane 1) and an increased degree of kethoxal modification at G22, G26, G27, and G28 (Figure S3B, lane 2 vs lane 1). Probe 9 is fully complementary to nucleotides 6−11. The binding of probe 9 to the RNA apparently breaks the double helix and leaves nucleotides 22−27 open for modification. Probe 8 probably causes a structural rearrangement similar to probe 9. The same NMIA modification experiment with probe 8 did not reveal any difference from the unmodified control (result not shown), however. This is likely because probe 8, 5′CUD^{L}GG^{L}G^{L}, has three consecutive guanosines, which may favor G-quadruplex formation in solution (*58*). Optical melting experiments showed that probe 8 at 10 μM in 135K/25Na/50HEPES/10Mg melted above 70 °C (data not shown). Evidently, quadruplex formation prevented probe 8 from binding to RNRspBs in solution.

RNase H Cleavage Induced by Antisense Oligodeoxyribonucleotides. The microarray and probe footprinting experiments suggested that design of antisense oligonucleotides and small interfering RNA (siRNA) for an RNA target with known secondary structure could be counterintuitive. For example, the long single strands J11/12 and J12/11 in RNRspBs are expected to be a good target for antisense DNA or siRNA. Microarray experiments, however, show that they may not bind to short probes and therefore may not be good targets. On the other hand, nucleotides near the 5′-terminus are expected to be poor targets because they are all base paired in the secondary structure. RNase H experiments were conducted to test whether results from isoenergetic microarrays provide guidance for choosing antisense DNA sequences.

As shown in Table S2 and Figure S4 of the Supporting Information, the strongest RNase H cleavages were induced by probes CC97−111, GC130−140, AT73−86, and AT20−32 (see Materials and Methods for the nomenclature). This does not correlate with either microarray binding or chemical modification. Because CC97−111 and GC130−140 cover all nucleotides in J11/12 and J12/11, respectively, they apparently break tertiary interactions in the internal loop. GC1−11 and TC1−13 induced only weak or moderate cleavage of the double-stranded region at the 5′-terminus and also induced cleavage at sites not completely complementary to the probe. Probe GT57−70 induced no clear cleavage.

DISCUSSION

The rapid discovery of many novel RNA functions has changed our understanding of the importance of RNA in life processes. RNA functions depend on secondary and tertiary structures. Determining RNA structures, determining structure−function relationships, and determining how to interfere with them are important steps in controlling RNA functions. Toward this end, computer programs have been developed to predict RNA structure from sequence (*59*−*62*) and the binding of oligonucleotides to folded RNA (*57*, *63*, *64*). Because of the extensive base pairing ability of nucleotides and the flexibility of the phosphate−ribose

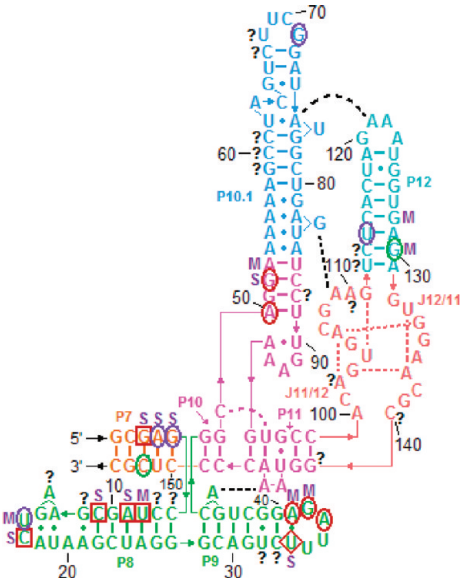

FIGURE 7: Unambiguous binding sites of RNRspBs by isoenergetic probes on a microarray explored in three buffer conditions. Red squares indicate strong binding in 140Na/80HEPES/10Mg and 135K/25Na/50HEPES/10Mg buffers. Red circles indicate intermediate binding in 140Na/80HEPES/10Mg and 135K/25Na/50HEPES/10Mg buffers. Purple circles indicate intermediate binding in 135K/25Na/50HEPES/10Mg buffer. The red diamond indicates intermediate binding in 140Na/80HEPES/10Mg buffer and strong binding in 135K/25Na/50HEPES/10Mg buffer. Green circles indicate intermediate binding in 140Na/80HEPES/10Mg buffer. S indicates strong binding in 135K/25Na/50HEPES/1MNa buffer. M indicates intermediate binding in 135K/25Na/50HEPES/1MNa. Question marks indicate ambiguous binding sites. Adapted from ref *22*.

backbone (*65*), however, RNA molecules have a large folding space. As a result, only a few classes of RNA secondary structures have been determined definitively by comparative sequence analysis or experimental methods such as NMR, crystallography, and chemical and enzymatic mapping (*19*−*27*). When tested against these structures, on average 70% of Watson−Crick and GU base pairs are contained in minimum free energy structures predicted by programs like RNAstructure (*51*) and MFOLD (*59*). Usually, the predictions can be improved when experimental constraints on paired or unpaired nucleotides are used to limit folding space (*19*, *51*, *66*). Oligonucleotide microarrays can rapidly generate a large amount of data that in principle could also be used to restrain RNA folding space (*36*−*38*). The results presented here, however, indicate that such applications will require an understanding of factors affecting probe binding that is more sophisticated than what is currently available. Such understanding should also inform the rational design of oligonucleotides to interfere with RNA function.

The RNA studied in this work, RNRspBs, has many unique features that can complicate probe binding and structure prediction. It contains many duplexes of only 2, 3, or 4 bp. A three-way multibranch loop and a four-way multibranch loop are separated only by the 2 bp stem of P10 at the core of the structure. Stem P11 has four Watson−Crick base pairs interrupted by an AA bulge loop and a GU wobble pair, and stem P11 separates the three-way multibranch loop from the large internal loop comprised of J11/12 and J12/11.

Implications for Structure Prediction. Even though RNRspBs has a complex structure, free energy minimization with or without chemical mapping constraints correctly predicts 79.5% of the known base pairs (Table 1). The incorrect base pairing occurs in the region flanking the two multibranch loops (Figure 3), a motif for which there is little information about the sequence dependence of stability. While chemical mapping constraints do not improve the predicted minimum free energy structure, they do eliminate many possible structures and raise the rank of a structure that is 93.2% accurate (Table 1). The calculations use free energy parameters determined in 1 M NaCl (*51*, *67*, *68*). The chemical mapping results, however, indicate that the secondary structure is the same in 135 mM K^+ with or without 10 mM Mg^{2+}. In addition, chemical mapping, microarray binding, and native PAGE results indicate that the secondary structure is the same in 135 mM K^+ with 10 mM Mg^{2+} or 1 M NaCl. Chemical mapping experiments with the cyclized *Tetrahymena* group I intron have also indicated similar secondary structure in the presence of 10 mM Mg^{2+} or 1 M Na^+ (*69*). Evidently, parameters measured in 1 M Na^+ provide reasonable approximations for other salt conditions.

Probe Binding Is Surprising. While the chemical mapping results are consistent with the known secondary structure, some of the microarray binding results are surprising. Three of the four hairpin loops bind probes as expected, but stems P7, P8, P10.1, and P12 bind probes unexpectedly (Figure 7). NMIA and kethoxal footprinting of probe 3 is consistent with strong binding to stem P7 inducing a rearrangement of stems P7 and P8, which results in formation of new base pairs, G22-C154, C23-G153, A25-U151, G26-C150, G27-C149, and perhaps G28-C148 (Figure S5 of the Supporting Information). Binding of probe 3 to rearranged RNRspBs has a predicted ΔG°_{37} of −6.5 kcal/mol. NMIA and kethoxal footprinting of probe 9 is consistent with strand invasion that breaks P8 (Figure S6 of the Supporting Information). Strand invasion is promoted by the favorable free energy of 3 or 4 kcal/mol provided by modifications in the probes. The overall binding free energy, ΔG°_{37}, is predicted to be −3.3 kcal/mol. This suggests that strand invasion and secondary structure rearrangement are easier than expected. Intramolecular rearrangement of secondary structure on a millisecond time scale has been observed for the 5′-leader sequence of *Leptomonas collosoa* (*70*).

The strong binding of probe 8 to RNRspBs is very surprising because strand invasion caused by probe 8 binding to nucleotides 6−10 in RNRspBs is predicted to be unfavorable with a ΔG°_{37} of 2.6 kcal/mol. Examination of the RNRspBs sequence for potential alternative binding sites, however, reveals that binding of probe 8 can become favorable in two situations: (1) binding to nucleotides 33−38 with a ΔG°_{37} of −5.6 kcal/mol and (2) binding to nucleotides 6−10 and 23−26, which is possible when probes are densely immobilized on the microarray and cause the breaking of P8.

The intermediate binding of probes 114 and 130 to stem P12 is surprising because in each case five intramolecular Watson−Crick pairs are likely broken. This binding could also induce structural rearrangements (Figure S7 of the Supporting Information). Moreover, the modifications in the probes are likely to make the probe-RNA base pairing more stable by at least 4 kcal/mol relative to completely Watson−Crick RNA-RNA base pairing (Figure S7) (*39*).

The intermediate binding of probes 50 and 52 probably requires breaking of four intramolecular base pairs. In these cases, a dramatic structural rearrangement may not be involved. Binding of probe 50 or 52 has the potential to break the 2 bp stem of P10 and thus merge the three-way and four-way junctions into a single five-way junction. On the basis of available parameters for junctions (*71*), the five-way junction is ~1 kcal/mol less destabilizing

than the combination of a three-way junction and a four-way junction. Probes 50 and 52 form five and six Watson−Crick base pairs, respectively, and their modifications add at least another three and four kcal/mol, respectively, of favorable free energy relative to the four broken RNA-RNA Watson−Crick pairs.

Salt Conditions Affect Probe Binding. As shown in Figure 6, probe binding relative to that of probe 17 depends somewhat on salt conditions. When compared to 135K/25Na/50HEPES/10Mg, probe 33(67) binds much less tightly in 140Na/80HEPES/10Mg, but more tightly in 135K/25Na/50HEPES/1MNa. If a cutoff of 0.2 is used to indicate significance, then binding in 140Na/80HEPES/10Mg is also weakened for probes 5, 6(60), 12, 16, and 32(112) but strengthened for probes 3, 7(61), and 88. Binding in 135K/25Na/50HEPES/1MNa is weakened for probes 12 and 114 but strengthened for probes 4, 5, 9, 34, 38, 39, 52, 59, 102, 128, and 130 in addition to 33(67). The ambiguity in binding sites of many of the probes (Table 2 and Figure 7) prohibits detailed interpretation. Nevertheless, it appears that binding to P7 and P8, which abut a multibranch loop, to the loop region of P9 and to P10.1 may depend on salt conditions. These are the regions with the densest clusters of probe binding. It is known that Na^+, K^+, and Mg^{2+} can affect the thermodynamic stabilities of various motifs (*52*, *72*−*75*).

Implications for the Design of Therapeutics. Many approaches are being developed to target RNA with oligonucleotide mimics as therapeutics (*14*, *15*). It would be advantageous to develop approaches that use short oligonucleotides (*76*, *77*). The results reported here suggest that the design of such oligonucleotides may not follow expected rules. For example, on the basis of known secondary structure, J11/12 and J12/11 are expected to be good targets. Only probes 102 and 110(14) potentially bind to J11/12, however, and both may bind elsewhere (Table 2). In contrast, probes are not expected to bind to double-helical regions but do bind to P7, P8, P10.1, and P12. While the limited knowledge of loop thermodynamics does not allow prediction of such binding, microarray experiments provide a rapid way to reveal them. The results suggest that short oligonucleotides may induce refolding of an RNA into an alternate conformation that could abrogate function.

CONCLUSIONS

Unexpected binding to an isoenergetic oligonucleotide microarray is observed for a target RNA composed of many short double-helical regions, large internal loops, and extensive tertiary interactions. Because of their enhanced binding free energies, isoenergetic probes can break short duplexes, merge adjacent loops, and/or induce refolding. This suggests new approaches to the rational design of short oligonucleotide therapeutics. For example, rational design can consider targeting short helical regions to induce refolding to an inactive conformation. Given the current limited knowledge of the energetics of RNA loops and tertiary interactions, however, microarray binding data do not provide a reliable check on secondary structures deduced from free energy minimization coupled with chemical modification constraints when the RNA has short helices and large loops. Results from chemical modification experiments, however, provide useful constraints on folding space. Results from chemical modification, microarray binding, and native PAGE indicate that the folding of the *B. subtilis* RNase P RNA specificity domain is similar in the presence of 1 M Na^+ or 10 mM Mg^{2+}.

ACKNOWLEDGMENT

We thank Prof. Alfonso Mondragón for the plasmid containing the gene for RNRspBs.

SUPPORTING INFORMATION AVAILABLE

Sources of materials used in the study; comparison of free energies between 2′-*O*-methyl RNA probes at 37 and 4 °C and corresponding isoenergetic probes at 37 °C as well as free energies of isoenergetic probes at alternative binding sites (Table S1); RNase H cleavages and intensities induced by oligodeoxyribonucleotides (Table S2); RNRspBs folded in buffers containing different metal ions resolved by native PAGE (Figure S1); comparison of predicted ΔG°_{37} values of isoenergetic probes, 2′-*O*-methyl probes, and 6-mer DNA probes bound to an unstructured RNA target (Figure S2); NMIA and kethoxal footprinting at 22 °C of RNRspBs binding sites for probe 3, 5′$CU^LCG^LCG^L$, and probe 9, 5′$GC^LUD^LGG^L$ (Figure S3); RNase H cleavage induced by antisense oligodeoxyribonucleotides (Figure S4); alternative binding of probe 3 to RNRspBs (Figure S5); strand invasion of probe 9 into P8 of RNRspBs (Figure S6); and possible local structural rearrangement of RNRspBs caused by binding of probe 114, 5′$U^LGD^LGD^LG^L$, or of probe 130, 5′$CUC^LUC^LG^L$ (Figure S7). This material is available free of charge via the Internet at http://pubs.acs.org.

REFERENCES

1. Reineke, L. C., Komar, A. A., Caprara, M. G., and Merrick, W. C. (2008) A small stem loop element directs internal initiation of the URE2 internal ribosome entry site in *Saccharomyces cerevisiae*. *J. Biol. Chem. 283*, 19011–19025.
2. Noller, H. F. (2005) RNA structure: Reading the ribosome. *Science 309*, 1508–1514.
3. Vasudevan, S., Tong, Y., and Steitz, J. A. (2007) Switching from repression to activation: MicroRNAs can up-regulate translation. *Science 318*, 1931–1934.
4. Masse, E., Majdalani, N., and Gottesman, S. (2003) Regulatory roles for small RNAs in bacteria. *Curr. Opin. Microbiol. 6*, 120–124.
5. Jones-Rhoades, M. W., Bartel, D. P., and Bartel, B. (2006) MicroRNAs and their regulatory roles in plants. *Annu. Rev. Plant Biol. 57*, 19–53.
6. Meister, G., Landthaler, M., Dorsett, Y., and Tuschl, T. (2004) Sequence-specific inhibition of microRNA- and siRNA-induced RNA silencing. *RNA 10*, 544–550.
7. Breaker, R. R. (2008) Complex riboswitches. *Science 319*, 1795–1797.
8. Ma, X., Yang, C., Alexandrov, A., Grayhack, E. J., Behm-Ansmant, I., and Yu, Y. T. (2005) Pseudouridylation of yeast U2 snRNA is catalyzed by either an RNA-guided or RNA-independent mechanism. *EMBO J. 24*, 2403–2413.
9. Tycowski, K. T., Aab, A., and Steitz, J. A. (2004) Guide RNAs with 5′ caps and novel box C/D snoRNA-like domains for modification of snRNAs in metazoa. *Curr. Biol. 14*, 1985–1995.
10. Goodier, J. L., and Kazazian, H. H., Jr. (2008) Retrotransposons revisited: The restraint and rehabilitation of parasites. *Cell 135*, 23–35.
11. Schimmel, P. (2008) An editing activity that prevents mistranslation and connection to disease. *J. Biol. Chem. 283*, 28777–28782.
12. Grimson, A., Srivastava, M., Fahey, B., Woodcroft, B. J., Chiang, H. R., King, N., Degnan, B. M., Rokhsar, D. S., and Bartel, D. P. (2008) Early origins and evolution of microRNAs and Piwi-interacting RNAs in animals. *Nature 455*, 1193–1197.
13. Coughlin, D. J., Pleiss, J. A., Walker, S. C., Whitworth, G. B., and Engelke, D. R. (2008) Genome-wide search for yeast RNase P substrates reveals role in maturation of intron-encoded box C/D small nucleolar RNAs. *Proc. Natl. Acad. Sci. U.S.A. 105*, 12218–12223.
14. Spurgers, K. B., Sharkey, C. M., Warfield, K. L., and Bavari, S. (2008) Oligonucleotide antiviral therapeutics: Antisense and RNA interference for highly pathogenic RNA viruses. *Antiviral Res. 78*, 26–36.
15. Drude, I., Dombos, V., Vauleon, S., and Muller, S. (2007) Drugs made of RNA: Development and application of engineered RNAs for gene therapy. *Mini Rev. Med. Chem. 7*, 912–931.

16. Tilesi, F., Fradiani, P., Socci, V., Willems, D., and Ascenzioni, F. (2009) Design and validation of siRNAs and shRNAs. *Curr. Opin. Mol. Ther. 11*, 156–164.
17. Lu, Z. J., and Mathews, D. H. (2008) OligoWalk: An online siRNA design tool utilizing hybridization thermodynamics. *Nucleic Acids Res. 36*, W104–W108.
18. Alkan, C., Karakoc, E., Nadeau, J. H., Sahinalp, S. C., and Zhang, K. (2006) RNA-RNA interaction prediction and antisense RNA target search. *J. Comput. Biol. 13*, 267–282.
19. Hart, J. M., Kennedy, S. D., Mathews, D. H., and Turner, D. H. (2008) NMR-assisted prediction of RNA secondary structure: Identification of a probable pseudoknot in the coding region of an R2 retrotransposon. *J. Am. Chem. Soc. 130*, 10233–10239.
20. Lukavsky, P. J., and Puglisi, J. D. (2005) Structure determination of large biological RNAs. *Methods Enzymol. 394*, 399–416.
21. D'Souza, V., Dey, A., Habib, D., and Summers, M. F. (2004) NMR structure of the 101-nucleotide core encapsidation signal of the Moloney murine leukemia virus. *J. Mol. Biol. 337*, 427–442.
22. Krasilnikov, A. S., Yang, X., Pan, T., and Mondragón, A. (2003) Crystal structure of the specificity domain of ribonuclease P. *Nature 421*, 760–764.
23. Kieft, J. S., Zhou, K., Grech, A., Jubin, R., and Doudna, J. A. (2002) Crystal structure of an RNA tertiary domain essential to HCV IRES-mediated translation initiation. *Nat. Struct. Biol. 9*, 370–374.
24. Ban, N., Nissen, P., Hanse, J., Moore, P. B., and Steitz, T. A. (2000) The complete atomic structure of the large ribosomal subunit at 2.4 Å resolution. *Science 289*, 905–920.
25. Cate, J. H., Gooding, A. R., Podell, E., Zhou, K., Golden, B. L., Kundrot, C. E., Cech, T. R., and Doudna, J. A. (1996) Crystal structure of a group I ribozyme domain: Principles of RNA packing. *Science 273*, 1678–1685.
26. Gutell, R. R., Lee, J. C., and Cannone, J. J. (2003) The accuracy of ribosomal RNA comparative structure models. *Curr. Opin. Struct. Biol. 12*, 301–310.
27. Pace, N. R., Thomas, B. C., and Woese, C. R. (1999) Probing RNA structure, function, and history by comparative analysis. The RNA World, 2nd ed., pp 113−141, Cold Spring Harbor Laboratory Press, Plainview, NY.
28. Bonetta, L. (2006) Genome sequencing in the fast lane. *Nat. Methods 3*, 141–147.
29. Mortimer, S. A., and Weeks, K. M. (2007) A fast-acting reagent for accurate analysis of RNA secondary and tertiary structure by SHAPE chemistry. *J. Am. Chem. Soc. 129*, 4144–4145.
30. Kauffmann, A. D., Campagna, R. J., Bartels, C. B., and Childs-Disney, J. L. (2009) Improvement of RNA secondary structure prediction using RNase H cleavage and randomized oligonucleotides. *Nucleic Acids Res. 37*, e121.
31. Ziehler, W. A., and Engelke, D. R. (2001) Probing RNA structure with chemical reagents and enzymes. Current Protocols in Nucleic Acid Chemistry, Chapter 6, Unit 6.1, Wiley-Interscience, Somerset, NJ.
32. Noller, H. F., and Chaires, J. B. (1972) Functional modification of 16S ribosomal RNA by kethoxal. *Proc. Natl. Acad. Sci. U.S.A. 69*, 3115–3118.
33. Ooms, M., Verhoef, K., Southern, E., Huthoff, H., and Berkhout, B. (2004) Probing alternative foldings of the HIV-1 leader RNA by antisense oligonucleotide scanning arrays. *Nucleic Acids Res. 32*, 819–827.
34. Sohail, M., Akhtar, S., and Southern, E. M. (1999) The folding of large RNAs studied by hybridization to arrays of complementary oligonucleotides. *RNA 5*, 646–655.
35. Mir, K. U., and Southern, E. M. (1999) Determining the influence of structure on hybridization using oligonucleotide arrays. *Nat. Biotechnol. 17*, 788–792.
36. Kierzek, E., Kierzek, R., Turner, D. H., and Catrina, I. E. (2006) Facilitating RNA structure prediction with microarrays. *Biochemistry 45*, 581–593.
37. Kierzek, E., Kierzek, R., Moss, W. N., Christensen, S. M., Eickbush, T. H., and Turner, D. H. (2008) Isoenergetic penta- and hexanucleotide microarray probing and chemical mapping provide a secondary structure model for an RNA element orchestrating R2 retrotransposon protein function. *Nucleic Acids Res. 36*, 1770–1782.
38. Kierzek, E., Christensen, S. M., Eickbush, T. H., Kierzek, R., Turner, D. H., and Moss, W. N. (2009) Secondary structures for 5′ regions of R2 retrotransposon RNAs reveal a novel conserved pseudoknot and regions that evolve under different constraints. *J. Mol. Biol. 390*, 428–442.
39. Pasternak, A., Kierzek, E., Pasternak, K., Turner, D. H., and Kierzek, R. (2007) A chemical synthesis of LNA-2,6-diaminopurine riboside, and the influence of 2′-O-methyl-2,6-diaminopurine and LNA-2,6-diaminopurine ribosides on the thermodynamic properties of 2′-O-methyl RNA/RNA heteroduplexes. *Nucleic Acids Res. 35*, 4055–4063.
40. Kierzek, E., Ciesielska, A., Pasternak, K., Mathews, D. H., Turner, D. H., and Kierzek, R. (2005) The influence of locked nucleic acid residues on the thermodynamic properties of 2′-O-methyl RNA/RNA heteroduplexes. *Nucleic Acids Res. 33*, 5082–5093.
41. Walker, S. C., and Engelke, D. R. (2006) Ribonuclease P: The evolution of an ancient RNA enzyme. *Crit. Rev. Biochem. Mol. Biol. 41*, 77–102.
42. Frank, D. N., and Pace, N. R. (1998) Ribonuclease P: Unity and diversity in a tRNA processing ribozyme. *Annu. Rev. Biochem. 67*, 153–180.
43. Guerrier-Takada, C., Gardiner, K., Marsh, T., Pace, N., and Altman, S. (1983) The RNA moiety of ribonuclease P is the catalytic subunit of the enzyme. *Cell 35*, 849–857.
44. Qin, H., Sosnick, T. R., and Pan, T. (2001) Modular construction of a tertiary RNA structure: The specificity domain of the *Bacillus subtilis* RNase P RNA. *Biochemistry 40*, 11202–11210.
45. Brown, J. W., Nolan, J. M., Haas, E. S., Rubio, M. A., Major, F., and Pace, N. R. (1996) Comparative analysis of ribonuclease P RNA using gene sequences from natural microbial populations reveals tertiary structural elements. *Proc. Natl. Acad. Sci. U.S.A. 93*, 3001–3006.
46. James, B. D., Olsen, G. J., Liu, J., and Pace, N. R. (1988) The secondary structure of ribonuclease P RNA, the catalytic element of a ribonucleoprotein enzyme. *Cell 52*, 19–26.
47. Matteucci, M. D., and Caruthers, M. H. (1981) Synthesis of deoxyoligonucleotides on a polymer support. *J. Am. Chem. Soc. 103*, 3185–3191.
48. Caruthers, M. H., Beaton, G., Wu, J. V., and Wiesler, W. (1992) Chemical synthesis of deoxyoligonucleotides and deoxyoligonucleotide analogs. *Methods Enzymol. 211*, 3–20.
49. Ausubel, F. M., Brent, R., Kingston, R. E., Moore, D. D., Seidman, J. G., Smith, J. A., and Struhl, K. (1991) Current Protocols in Molecular Biology, Chapter 1.7, Wiley-Interscience, Somerset, NJ.
50. Afanassiev, V., Hanemann, V., and Wölfl, S. (2000) Preparation of DNA and protein micro arrays on glass slides coated with an agarose film. *Nucleic Acids Res. 28*, e66.
51. Mathews, D. H., Disney, M. D., Childs, J. L., Schroeder, S. J., Zuker, M., and Turner, D. H. (2004) Incorporating chemical modification constraints into a dynamic programming algorithm for prediction of RNA secondary structure. *Proc. Natl. Acad. Sci. U.S.A. 101*, 7287–7292.
52. Draper, D. E., Grilley, D., and Soto, A. M. (2005) Ions and RNA folding. *Annu. Rev. Biophys. Biomol. Struct. 34*, 221–243.
53. Qu, X., Smith, G. J., Lee, K. T., Sosnick, T. R., Pan, T., and Scherer, N. F. (2008) Single-molecule nonequilibrium periodic Mg^{2+}-concentration jump experiments reveal details of the early folding pathways of a large RNA. *Proc. Natl. Acad. Sci. U.S.A. 105*, 6602–6607.
54. Fang, X., Littrell, K., Yang, X. J., Henderson, S. J., Siefert, S., Thiyagarajan, P., Pan, T., and Sosnick, T. R. (2000) Mg^{2+}-dependent compaction and folding of yeast tRNAPhe and the catalytic domain of the *B. subtilis* RNase P RNA determined by small-angle X-ray scattering. *Biochemistry 39*, 11107–11113.
55. Mathews, D. H. (2004) Using an RNA secondary structure partition function to determine confidence in base pairs predicted by free energy minimization. *RNA 10*, 1178–1190.
56. Pasternak, A., Kierzek, E., Pasternak, K., Fratczak, A., Turner, D. H., and Kierzek, R. (2008) The thermodynamics of 3′-terminal pyrene and guanosine for the design of isoenergetic 2′-*O*-methyl-RNA-LNA chimeric oligonucleotide probes of RNA structure. *Biochemistry 47*, 1249–1258.
57. Mathews, D. H., Burkard, M. E., Freier, S. M., Wyatt, J. R., and Turner, D. H. (1999) Predicting oligonucleotide affinity to nucleic acid targets. *RNA 5*, 1458–1469.
58. Kim, J., Cheong, C., and Moore, P. B. (1991) Tetramerization of an RNA oligonucleotide containing a GGGG sequence. *Nature 351*, 331–332.
59. Zuker, M. (1989) On finding all suboptimal foldings of an RNA molecule. *Science 244*, 48–52.
60. Wuchty, S., Fontana, W., Hofacker, I. L., and Schuster, P. (1999) Complete suboptimal folding of RNA and the stability of secondary structures. *Biopolymers 49*, 146–165.
61. Do, C. B., Woods, D. A., and Batzoglou, S. (2006) CONTRAfold: RNA secondary structure prediction without physics-based models. *Bioinformatics 22*, e90–e98.
62. Ding, Y., Chan, C. Y., and Lawrence, C. E. (2004) Sfold web server for statistical folding and rational design of nucleic acids. *Nucleic Acids Res. 32*, W135–W141.

63. Matveeva, O. V., Mathews, D. H., Tsodikov, A. D., Shabalina, S. A., Gesteland, R. F., Atkins, J. F., and Freier, S. M. (2003) Thermodynamic criteria for high hit rate antisense oligonucleotide design. *Nucleic Acids Res. 31*, 4989–4994.
64. Ding, Y., and Lawrence, C. E. (2001) Statistical prediction of single-stranded regions in RNA secondary structure and application to predicting effective antisense target sites and beyond. *Nucleic Acids Res. 29*, 1034–1046.
65. Richardson, J. S., Schneider, B., Murray, L. W., Kapral, G. J., Immormino, R. M., Headd, J. J., Richardson, D. C., Ham, D., Hershkovits, E., Williams, L. D., Keating, K. S., Pyle, A. M., Micallef, D., Westbrook, J., and Berman, H. M. (2008) RNA backbone: Consensus all-angle conformers and modular string nomenclature (an RNA Ontology Consortium contribution). *RNA 14*, 465–481.
66. Deigan, K. E., Li, T. W., Mathews, D. H., and Weeks, K. M. (2009) Accurate SHAPE-directed RNA structure determination. *Proc. Natl. Acad. Sci. U.S.A. 106*, 97–102.
67. Turner, D. H. (2000) Conformational changes. Nucleic Acids: Structures, Properties, and Functions (Bloomfiled, V. A., Crothers, D. M., and Tinoco, I., Jr., Eds.) Chapter 8, pp 259−334, University Science Books, Sausalito, CA.
68. Xia, T., SantaLucia, J., Jr., Burkard, M. E., Kierzek, R., Schroeder, S. J., Jiao, X., Cox, C., and Turner, D. H. (1998) Thermodynamic parameters for an expanded nearest-neighbor model for formation of RNA duplexes with Watson-Crick base pairs. *Biochemistry 37*, 14719–14735.
69. Jaeger, J. A., Zuker, M., and Turner, D. H. (1990) Melting and chemical modification of a cyclized self-splicing group I intron: Similarity of structures in 1 M Na^+, in 10 mM Mg^{2+}, and in the presence of substrate. *Biochemistry 29*, 10147–10158.
70. LeCuyer, K. A., and Crothers, D. M. (1994) Kinetics of an RNA conformational switch. *Proc. Natl. Acad. Sci. U.S.A. 91*, 3373–3377.
71. Mathews, D. H., and Turner, D. H. (2002) Experimentally derived nearest-neighbor parameters for the stability of RNA three- and four-way multibranch loops. *Biochemistry 41*, 869–880.
72. Misra, V. K., and Draper, D. E. (1998) On the role of magnesium ions in RNA stability. *Biopolymers 48*, 113–135.
73. Serra, M. J., Baird, J. D., Dale, T., Fey, B. L., Retatagos, K., and Westhof, E. (2002) Effects of magnesium ions on the stabilization of RNA oligomers of defined structures. *RNA 8*, 307–323.
74. Basu, S., Rambo, R. P., Strauss-Soukup, J., Cate, J. H., Ferre-D'Amare, A. R., Strobel, S. A., and Doudna, J. A. (1998) A specific monovalent metal ion integral to the AA platform of the RNA tetraloop receptor. *Nat. Struct. Biol. 5*, 986–992.
75. Vieregg, J., Cheng, W., Bustamante, C., and Tinoco, I., Jr. (2007) Measurement of the effect of monovalent cations on RNA hairpin stability. *J. Am. Chem. Soc. 129*, 14966–14973.
76. Testa, S. M., Gryaznov, S. M., and Turner, D. H. (1999) *In vitro* suicide inhibition of self-splicing of a group I intron from *Pneumocystis carinii* by an *N*3′→*P*5′ phosphoramidate hexanucleotide. *Proc. Natl. Acad. Sci. U.S.A. 96*, 2734–2739.
77. Childs, J. L., Disney, M. D., and Turner, D. H. (2002) Oligonucleotide directed misfolding of RNA inhibits *Candida albicans* group I intron splicing. *Proc. Natl. Acad. Sci. U.S.A. 99*, 11091–11096.